

# In Situ SAXS Study on a New Mechanism for Mesopore Formation of Ordered Mesoporous Carbons: Thermally Induced Self-Assembly

Jörg Schuster,<sup>†</sup> Ralf Köhn,<sup>‡</sup> Markus Döblinger,<sup>†</sup> Andreas Keilbach,<sup>†</sup> Heinz Amenitsch,<sup>§</sup> and Thomas Bein<sup>\*,†</sup>

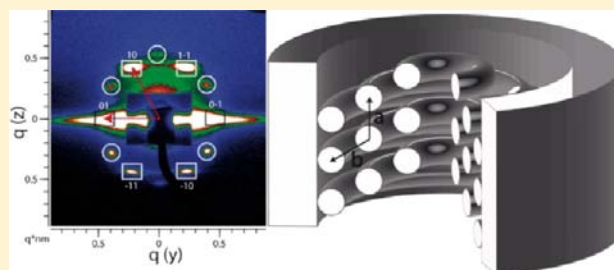
<sup>†</sup>Department of Chemistry and Center for NanoScience (CeNS), University of Munich (LMU), Butenandtstraße 5-13 (Gerhard-Ertl Building), 81377 Munich, Germany

<sup>‡</sup>Center for Free-Electron Laser Science, Notkestrasse 85, 22607 Hamburg, Germany

<sup>§</sup>Institute of Biophysics and Nanosystems Research, Austrian Academy of Sciences, Schmiedlstraße 6, 8042 Graz, Austria

## Supporting Information

**ABSTRACT:** A new mechanism for mesostructure formation of ordered mesoporous carbons (OMCs) was investigated with in situ small-angle X-ray scattering (SAXS) measurements: thermally induced self-assembly. Unlike the well-established evaporation-induced self-assembly (EISA), the structure formation for organic–organic self-assembly of an oligomeric resol precursor and the block-copolymer templates Pluronic P123 and F127 does not occur during evaporation but only by following a thermopolymerization step at temperatures above 100 °C. The systems investigated here were cubic ( $Im\bar{3}m$ ), orthorhombic  $Fmmm$  and 2D-hexagonal (plane group  $p6mm$ ) mesoporous carbon phases in confined environments, as thin films and within the pores of anodic alumina membranes (AAMs), respectively. The thin films were prepared by spin-coating mixtures of the resol precursor and the surfactants in ethanol followed by thermopolymerization of the precursor oligomers. The carbon phases within the pores of AAMs were made by imbibition of the latter solutions followed by solvent evaporation and thermopolymerization within the solid template. This thermopolymerization step was investigated in detail with in situ grazing incidence small-angle X-ray scattering (GISAXS, for films) and in situ SAXS (for AAMs). It was found that the structural evolution strongly depends on the chosen temperature, which controls both the rate of the mesostructure formation and the spatial dimensions of the resulting mesophase. Therefore the process of structure formation differs significantly from the known EISA process and may rather be viewed as thermally induced self-assembly. The complete process of structure formation, template removal, and shrinkage during carbonization up to 1100 °C was monitored in this in situ SAXS study.



## INTRODUCTION

Porous carbon materials are essential for many modern applications. They are employed as electrode materials for batteries, supercapacitors, and fuel cells, as sorbents for separation and gas storage or as catalyst supports due to their favorable properties including high specific surface area and pore volume, chemical inertness, and electrical conductivity.

Conventional activated carbons presently in use typically consist of disordered microporous amorphous carbon. The main drawback of these activated microporous carbons is limited accessibility and mass transport within the micropores.<sup>1</sup> Ordered mesoporous carbons (OMC),<sup>1–3</sup> tailor-made in terms of morphology and properties of the periodic mesopore system, could be beneficial for several of the aforementioned applications. Ordered mesoporous carbon in bulk or powder form is commonly synthesized either by hard templating,<sup>4–8</sup> where periodic mesoporous silica is filled with carbon precursors followed by carbonization and removal of the silica, or by soft templating,<sup>9–11</sup> using the self-assembly of soluble

carbon precursors with liquid crystalline phases of surfactants or block copolymers acting as soft templates.

The examples for mesoporous carbon thin films<sup>12–16</sup> or phases still embedded in alumina membrane (AAM) hosts<sup>17–23</sup> are limited to soft-templating methods. Hard-templating methods for ordered mesoporous carbon based on porous silica templates have yet not been implemented for these morphologies, which is mainly attributed to weak adhesion of the resulting carbon material to the substrate after etching of the silica template.<sup>13,24</sup> The few examples using hard templating of mesoporous silica for AAMs result either in mesostructured carbon/silica composites<sup>4,24</sup> and/or in freestanding fibers.<sup>24</sup> An alternative approach for mesoporous carbon films uses spin coating of sucrose and silica nanoparticles and subsequent removal of the silica.<sup>25</sup> However, these films contained a disordered pore system. While the final carbon structure

Received: September 22, 2011

Published: May 19, 2012

obtained via hard templating is controlled by the solid template, the final structures made by soft templating are much more sensitive to experimental conditions, such as concentrations, temperature, or humidity, during structure formation. Therefore, the understanding and control of structure formation processes for soft-templating methods concerning mesostructural symmetry, morphology, and orientation of the desired mesoporous carbon phases are essential, especially for syntheses in confined environments.

In situ grazing incidence small-angle X-ray scattering (GISAXS) characterization of thin films and in situ small-angle X-ray scattering (SAXS) of AAM/OMC composites are powerful tools to investigate structural changes during all steps of structure formation and processing—self-assembly, template removal, and the final carbonization. Some examples for in situ SAXS studies regarding the structure formation with evaporation-induced self-assembly (EISA)<sup>26–28</sup> and thermal processing<sup>29,30</sup> of mesoporous systems other than mesoporous carbon have already been reported.

The self-assembly mechanisms for OMC materials made by soft-templating have not yet been investigated in detail. Liang et al.<sup>12</sup> described the self-assembly of a polystyrene-*b*-poly(4-vinylpyridine) block copolymer (PS-P4VP) with resorcinol and formaldehyde as carbon sources, as solvent-induced self-assembly. For other OMC systems, mainly for the popular resol-Pluronic system,<sup>1,9,15,31–34</sup> the structure formation is mostly described as an EISA process, such as for mesostructured metal oxides (e.g., silica<sup>26</sup> or titania)<sup>30</sup> followed by a thermopolymerization step to cross-link the precursor oligomers.

For pure block copolymer films, there are examples for thermally induced self-assembly. Russell et al.<sup>35</sup> describe a thermal approach to get ordered block copolymers by annealing poly[(styrene-*r*-BCB)-*b*-lactic acid] (PSBCB-*b*-PLA) at 170 °C. Hawker and Kramer<sup>36</sup> show the synthesis of polymeric bicontinuous morphologies that were created by thermally annealing mixtures of poly(styrene-*b*-2-vinylpyridine) (PS-*b*-P2VP) block copolymers stabilized by Au-core/Pt-shell (Au\_Pt) nanoparticles. The self-assembly of block copolymers to form ordered nanostructured phases, also called microphase separation, is thermodynamically governed by the segregation strength of the different blocks.<sup>37–39</sup> The segregation strength can be described by the product  $\chi N$ , where  $\chi$  is the Flory–Huggins interaction parameter between segments of the differing blocks and  $N$  is the total number of repeated units. For Pluronic P123 and F127 used in this work, the segregation strength is not high enough to meet the critical values, and the polymers remain disordered. Watkins et al. showed that the critical segregation strength of Pluronic block copolymers (poly(ethylene oxide-propylene oxide-ethylene oxide)) could be exceeded by addition of polymers of variable length<sup>27</sup> or small molecules,<sup>28</sup> and nanostructured films were formed. Herein we report an in situ SAXS study on a new mechanism for mesostructure formation of OMCs in the form of thin films and confined within the pores of anodic alumina membranes: thermally induced self-assembly.

The OMC phases were obtained by solvent evaporation of mixtures of a preformed oligomeric resol precursor and the triblock copolymer templates Pluronic P123 and F127, respectively, followed by a thermopolymerization step at intermediate temperatures ( $\geq 100$  °C), and finally carbonization at high temperatures ( $\geq 600$  °C) in inert atmosphere. We found that unlike in the case of mesostructured metal oxides and also

different to literature on those soft-templated OMCs, the structure formation in these systems does not occur during evaporation of the solvent but during the thermopolymerization step and should, therefore, rather be called thermally induced self-assembly. As a consequence, the mesostructure is still flexible and can be controlled during the thermopolymerization step. Different thermopolymerization temperatures resulted in changed unit cell parameters for the final OMC structures. Template removal and carbonization of thin films and AAM composites were monitored up to 1100 °C, with mesopore order still retained at this temperature. We observed strong structural distortion for the thin films due to anisotropic shrinkage upon carbonization, but no distortion was found for the AAM composites due to the restricted shrinkage effect of the confining alumina wall.

## ■ EXPERIMENTAL SECTION

**Chemicals.** Formalin (37 wt % formaldehyde in water) and the triblock copolymers Pluronic P123 ( $M_w = 5800$ , EO<sub>20</sub>-PO<sub>70</sub>-EO<sub>20</sub>) and Pluronic F127 ( $M_w = 12\,600$ , EO<sub>106</sub>-PO<sub>70</sub>-EO<sub>106</sub>) were purchased from BASF AG. Phenol was obtained from Merck KGaA. All chemicals were used without further purification. Whatman anodiscs (25 and 47 mm diameter, nominal pore diameter 0.02  $\mu\text{m}$ ) were used as porous alumina substrates. Silicon wafers were kindly donated by Siltronic AG.

**Synthesis. Resol Precursor.** A low molecular weight precursor for the organic framework was synthesized in a reaction of phenol and formaldehyde in a base-catalyzed process according to Meng et al.<sup>9</sup> The molecular weight average of the resol precursor is expected to be smaller than 500 g/mol. For the synthesis, 6.1 g of phenol (0.064 mol) was molten in a flask with 1.3 g of 20 wt % sodium hydroxide solution (0.0065 mol). The mixture was heated up to 50 °C, and then 10.5 g of formalin (37 wt % formaldehyde in water, 0.1295 mol) was added dropwise. The molar ratio of phenol:formaldehyde:NaOH was 1:2:0.1. The clear, lightly yellow colored solution was stirred at 75 °C for 1 h and then cooled down to room temperature. The precursor solution was neutralized with 1 M hydrochloric acid, and the water was removed by vacuum evaporation below 50 °C. The resulting product was redissolved in ethanol to a total weight of 50 g.

**SDA Solutions.** Pluronic F127: 1.00 g of F127 (0.08 mmol) was dissolved in 20.0 g (0.45 mol) ethanol to give a 4.76 wt % solution. Pluronic P123: 1.00 g of P123 (0.17 mmol) was dissolved in 20.0 g (0.45 mol) ethanol to give a 4.76 wt % solution. For a double concentrated (9.52 wt %) template solution, 1.00 g of P123 (0.17 mmol) was dissolved in 9.5 g ethanol.

**Synthesis of Mesoporous Polymer and Carbon Films with 2D-Hexagonal Structure.**<sup>14</sup> 2D-hexagonal films were prepared with a molar ratio of phenol:formaldehyde:NaOH:P123 = 1:2:0.1:0.0063, which is equivalent to a weight ratio of the SDA (4.76 wt % P123) and precursor solution of 1:1. In a typical preparation, 1 g of the precursor solution was mixed with 1 g template solution (molar ratio phenol:formaldehyde:NaOH:P123 = 1:2:0.1:0.0063). After stirring for 10 min, a homogeneous solution was obtained. The mesostructured films were synthesized on polished silicon wafers. The wafers were cut into smaller pieces, washed with ethanol, and cleaned in an oxygen plasma for 1 min. The mixed precursor and SDA solutions were dropped on the wafers (ca. 2  $\times$  2 cm) through a syringe filter (CHROMAFIL PET-20/15 MS, pore size 0.20  $\mu\text{m}$ ) until they were completely covered and spin coated at 3000 rpm with an acceleration of 1260 rpm/s.

**Synthesis of Mesoporous Polymer and Carbon Films with Orthorhombic Structure.** Orthorhombic films were obtained with a molar ratio of phenol:formaldehyde:NaOH:P123 = 1:2:0.1:0.0029, which is equivalent to a weight ratio of the SDA (4.76 wt % F127) and precursor solution of 1:1. In a typical preparation, 1 g of the precursor solution was mixed with 1 g template solution (molar ratio phenol:formaldehyde:NaOH:P123 = 1:2:0.1:0.0063). For these films the same procedure as described above for solvent evaporation during spin coating was performed.

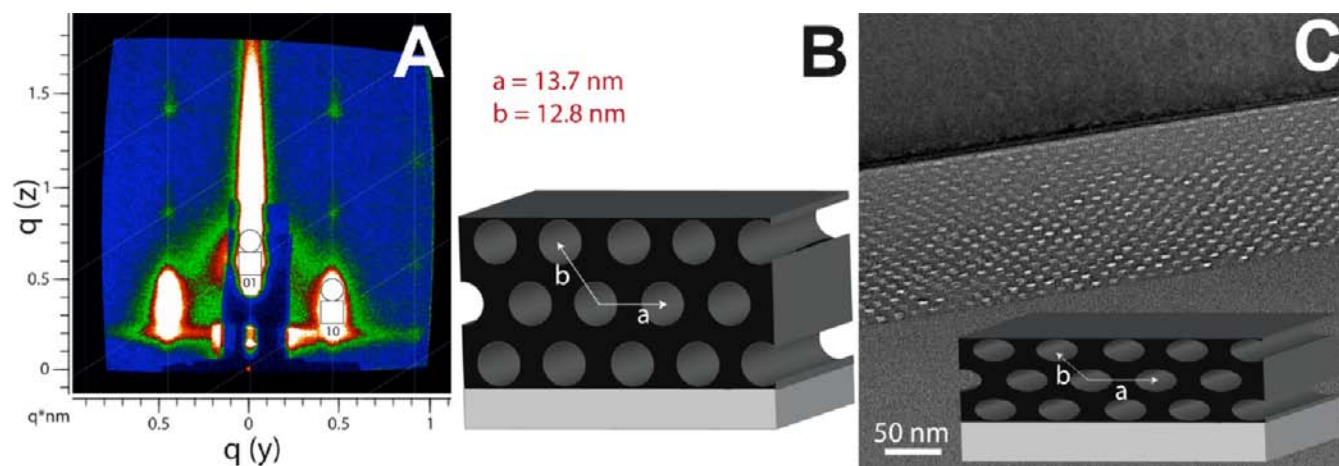


**Figure 1.** (A) GISAXS pattern of Film-Hex-110 visualizing the reciprocal lattice of a 2D-hexagonal structure, the peaks are indexed in the 2D-hexagonal unit cell (B,  $p6mm$ ), with the (01) plane parallel to the substrate. The most intense reflections are doubled due to the grazing incidence geometry, the lower reflection (squares) results from Bragg diffraction, and the second reflection on top of the first one (circles) is a specular reflection of the corresponding Bragg reflection. (C) TEM cross-section after pyrolysis at 400 °C, the inset displays the elliptically shaped pores of the distorted 2D-hexagonal structure due to uniaxial shrinkage.

**Synthesis of Mesoporous Polymer Resin and Carbon in AAMs with Circular Hexagonal Structure.**<sup>23</sup> The circular hexagonal phase was obtained for a molar ratio of phenol:formaldehyde:NaOH:P123 = 1:2:0.1:0.0095, which is equivalent to a weight ratio of the SDA (9.52 wt % P123) and precursor solution of 0.75:1. In a typical preparation, 1 g of the precursor solution was mixed with 0.75 g template solution. After stirring for 10 min, a homogeneous solution was obtained. The mixed solutions—0.75 mL for the 47 mm membrane and 0.25 mL for the 25 mm membrane, respectively—were spread over the membrane, followed by evaporation of the solvent overnight.

**Synthesis of Mesoporous Polymer Resin and Carbon in AAMs with Cubic Structure.**<sup>23</sup> The cubic phase was obtained for a molar ratio of phenol:formaldehyde:NaOH:F127 = 1:2:0.1:0.0044, which is equivalent to a weight ratio of the SDA and precursor solution of 1.5:1. In a typical preparation, 1 g of the precursor solution was mixed with 1.5 g template solution. For these membranes the same procedure of solvent evaporation was performed as described for the hexagonal structure.

**Thermopolymerization.** The solvent evaporation was followed by thermopolymerization at temperatures between 90 and 180 °C on a Anton Paar DHS 1100 heating plate until strong reflections were visible in the in situ recorded GISAXS patterns.

**Carbonization.** After thermopolymerization the samples were heated in the Anton Paar DHS 1100 heating chamber in nitrogen atmosphere with a ramp of 6 °C/min up to the defined limit of 1100 °C.

**Nomenclature.** The thin films are denoted Film-S-T, and the AAMs are denoted AAM-S-T. S represents the structure, -Hex for the hexagonal, -Or for orthorhombic, and -Cub for the cubic phase. T represents the thermopolymerization temperature reached at a ramp of 20 °C/min. For example AAM-Hex-110 is a composite with circular hexagonal structure, heated with a ramp of 20 °C/min and to the thermopolymerization temperature of 110 °C. Samples thermopolymerized using a faster ramp of 100 °C/min get the suffix fast, e.g., Film-Hex-180fast.

## ■ CHARACTERIZATION

GISAXS and SAXS experiments were performed at beamline BL 5.2 L<sup>40</sup> at Sincrotrone Elettra (Trieste, Italy). The wavelength of the incident beam was 0.15498 nm (8 keV), and the sample–detector distance was set to about 1.5 m for each of the different sessions. The samples were heated in a Anton Paar DHS 1100 heating chamber. The films were measured with GISAXS at incident angles of 0.3°. The film thickness is around

200 nm after thermopolymerization for all samples.<sup>14</sup> The incident angle of the GISAXS setup was relatively high (0.3°) as compared to Bang et al.,<sup>40</sup> thus the X-rays should penetrate the full film thickness. Doubling of reflections in z-direction arises from diffraction of the reflected incident beam.<sup>41</sup> As a result it sometimes seems that the reflections are strongly elongated along the z-axis, however the two reflections can be easily distinguished. The AAMs were measured with SAXS in transmission at an incident angle of 5°. For this purpose they were placed on a grooved copper plate (groove width 0.5 cm, depth 0.5 cm) on top of the heating plate. For temperatures above 200 °C the DHS 1100 was equipped with the provided graphite dome or with a self-made top, which consists of a rectangular steel tube with windows made from a 10 μm thin polyethylene terephthalate film (Kalle GmbH, Wiesbaden, Germany). The film was found to have a negligible contribution to the measured signal in contrast to the graphite dome, which produces an intense diffuse background at small angles. The sample temperature was verified with the phase transition of quartz at 573 °C.<sup>42,43</sup> The quartz jump was determined by a peak shift of the 101 reflection (Figure S1, Supporting Information). For this purpose, quartz crystals were placed on an AAM on top of the grooved copper plate. The set temperature at the phase transition was 569 °C, thus 4 °C (<1% error) lower than the real sample temperature. For radial intensity integrations of GISAXS patterns, the in-plane intensity (meaning intensity on the vertical axis) was masked according to Figure S2A, Supporting Information. For carbonization experiments using the aforementioned graphite dome, both in-plane intensity and scattering from the dome were masked according to Figure S2B, Supporting Information.

## ■ RESULTS AND DISCUSSION

**Mesoporous Structures.** Four OMC systems—two thin films and two in AAMs—were investigated in this in situ SAXS study. The thin films were obtained through organic–organic self-assembly of a preformed oligomeric resol precursor and triblock copolymer templates, which resulted in hexagonal (for Pluronic P123) and orthorhombic (for Pluronic F127) mesostructures, respectively. The 2D-hexagonal (plane group,  $p6mm$ ) mesoporous carbon thin films have already been

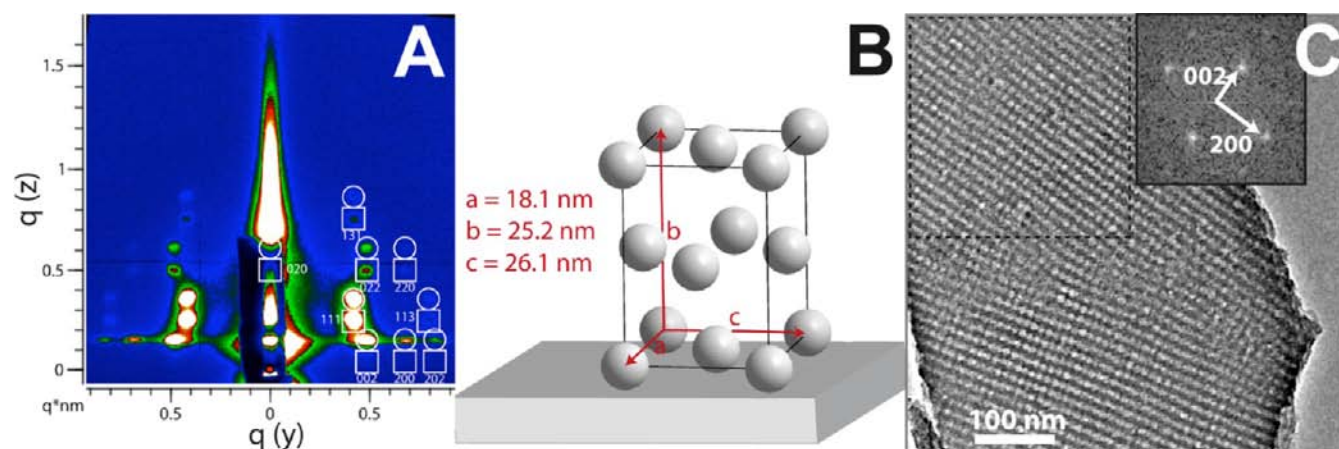


**Figure 2.** (A) GISAXS pattern of Film-Or-100 indexed according to the face-centered orthorhombic unit cell (B,  $Fm\bar{m}m$ ), with (010) plane parallel to the substrate. The most intense reflections are doubled due to the grazing incidence geometry—the lower reflection (squares) results from Bragg diffraction, and the second reflection on top of the first one (circles) is a specular reflection of the corresponding Bragg reflection. (C) TEM image after pyrolysis at 500 °C of a scratched off film in plan view, i.e., viewed along [010] of the orthorhombic structure with  $Fm\bar{m}m$  symmetry. The inset shows the Fourier transform of the area marked by a square. It is indexed according to the orthorhombic unit cell.

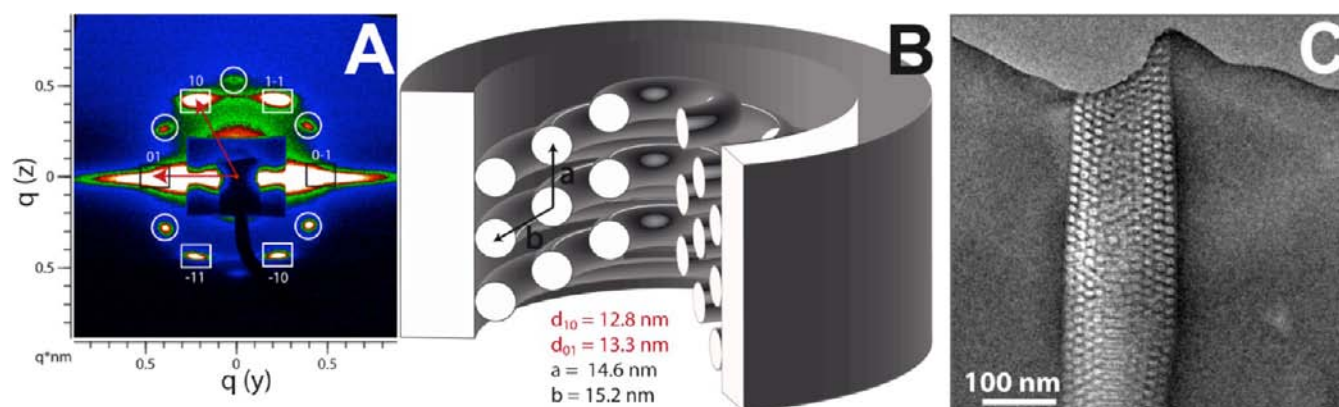


**Figure 3.** (A) SAXS pattern for the sample AAM-Hex-160 indexed in the circular hexagonal ( $p6mm$ ) unit cell (B). The squares show the reflections from the mesophases in the AAM pores, while the circles show reflections from a top layer on the membrane. (C) TEM cross-section after pyrolysis at 400 °C.

investigated in a combined GISAXS and TEM study.<sup>14</sup> Their structure can be described by cylindrical pores arranged in a hexagonal stacking parallel to the substrate. Figure 1A shows a typical GISAXS pattern for the 2D-hexagonal thin films, denoted as Film-Hex-T. All reflections lie on the reciprocal lattice of a 2D-hexagonal unit cell with the (01) plane parallel to the substrate. The TEM cross-section in Figure 1C shows the film after pyrolysis at 400 °C. The initial 2D-hexagonal structure with  $p6mm$  symmetry is distorted due to uniaxial shrinkage, which results in the plane group  $c2mm$ . In projection along the columns the pore shape becomes elliptical, which is illustrated by the inset of the TEM cross-section.

A typical GISAXS pattern for the orthorhombic thin films, denoted as Film-Or-T, is depicted in Figure 2A. The pattern shows a differing arrangement of reflections compared to the 2D-hexagonal structure that can be indexed according to a face-centered orthorhombic unit cell ( $Fm\bar{m}m$ ) with the (010) plane parallel to the substrate. Films possessing the above space group and orientation with respect to the substrate were already reported for carbon and metal oxides.<sup>13,16,29,44</sup> OMC phases synthesized with the surfactant Pluronic F127 usually show cubic  $Im\bar{3}m$  symmetry, but this can be changed to an orthorhombic  $Fm\bar{m}m$  symmetry due to distortion. The

symmetry change from cubic  $Im\bar{3}m$  to orthorhombic  $Fm\bar{m}m$  is also described by Falcaro<sup>29</sup> and Feng.<sup>34</sup> Figure 2C shows a TEM image of the film in plan view after pyrolysis at 500 °C, i.e., viewed along the [010] zone axis of the orthorhombic structure. Due to uniaxial shrinkage, the unit cell only shrunk along this axis (only  $b$  changes), therefore the dimensions observed in the TEM plan view ( $a$  and  $c$ ) are still in good agreement with the GISAXS pattern (Figure 2A) directly after thermopolymerization.

Circular hexagonal and cubic AAM phases, denoted as AAM-Hex-T and AAM-Cub-T, were obtained by organic–organic self-assembly of a preformed oligomeric resol precursor and the triblock copolymer templates Pluronic P123 (hexagonal) and Pluronic F127 (cubic), respectively. These mesostructures have been investigated before by combined SAXS and TEM.<sup>23</sup> Solvent casting and evaporation were followed by self-assembly and by thermopolymerization of the precursor oligomers, resulting in the mesostructured phenolic resin phases. A typical SAXS pattern for the circular hexagonal structure is presented in Figure 3A for the sample AAM-Hex-160. It can be indexed according to a zone axis parallel to the hexagonal axis of the unit cell (plane group  $p6mm$ , Figure 3B) with  $[2\bar{1}]$  orientation regarding the membrane normal. The hexagonal unit cell is

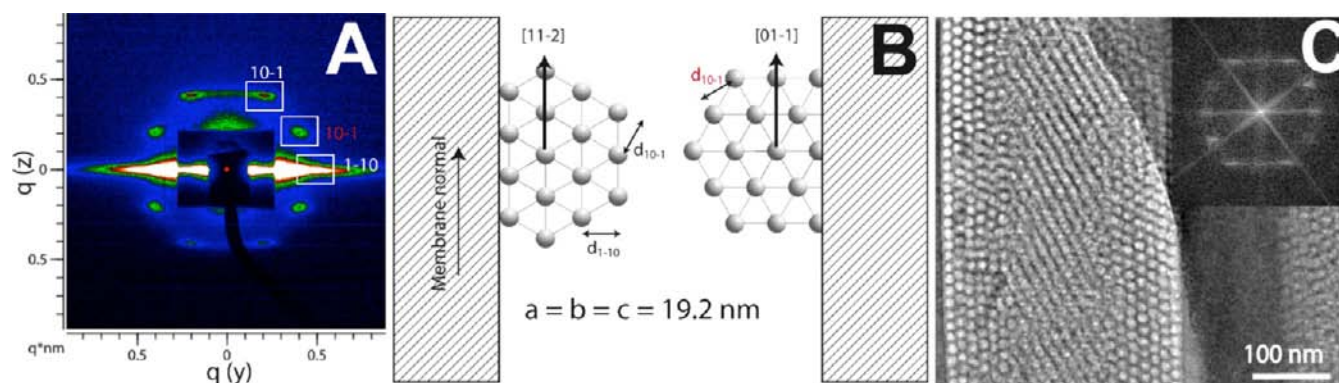


**Figure 4.** (A) SAXS pattern for the sample AAM-Cub-180 indexed in the cubic unit cell ( $Im\bar{3}m$ ). (B) Corresponding unit cell viewed along  $[111]$  and its possible orientations along the membrane normal,  $[11\bar{2}]$  and  $[01\bar{1}]$ . (C) TEM cross-section after pyrolysis at  $400\text{ }^{\circ}\text{C}$  with an FFT inset.

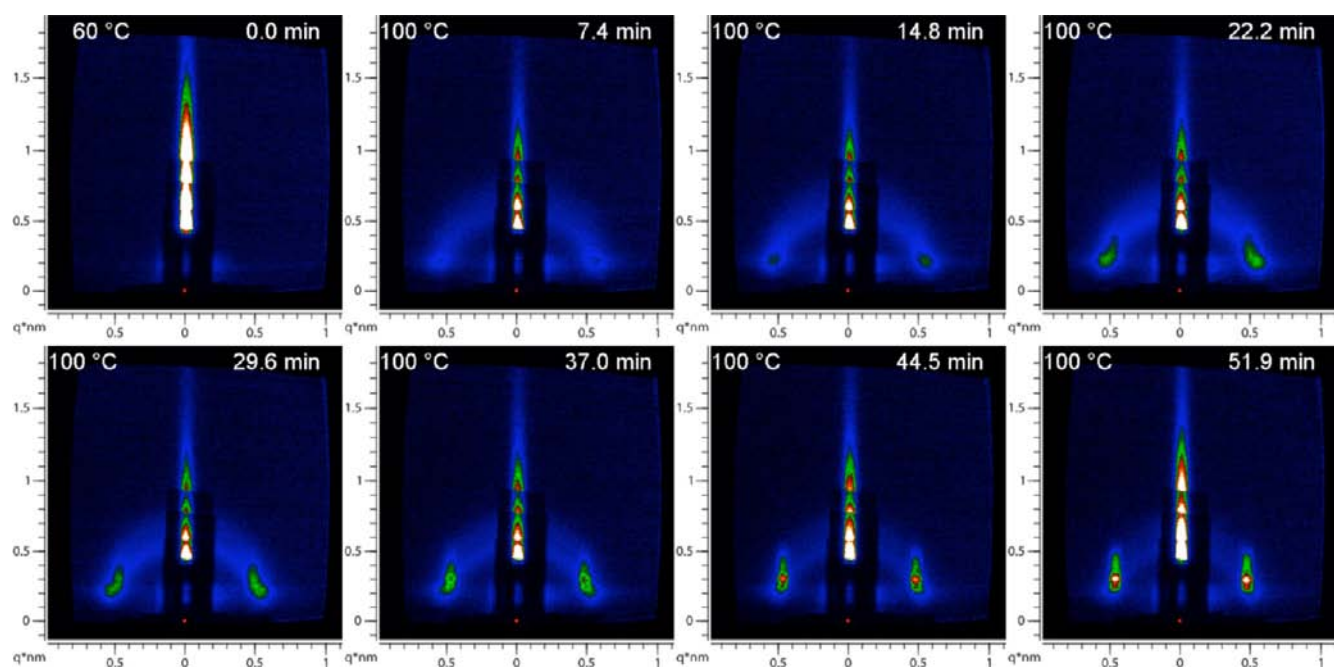


**Figure 5.** In situ GISAXS of Film-Hex-100: Structure formation during thermopolymerization at  $100\text{ }^{\circ}\text{C}$ .

slightly distorted as shown in the unit cell constants in Figure 3B. The squares show the reflections from the mesophases in the AAM pores, while the circles show reflections from a top layer on the membrane. This top layer also shows a 2D-hexagonal structure but with  $[01]$  orientation parallel to the membrane normal. The circular hexagonal mesoporous structure can also be observed in the TEM cross-section in Figure 3C after pyrolysis at  $400\text{ }^{\circ}\text{C}$ . Due to strong adhesion of the carbon to the AAM walls, a restricted shrinkage effect occurs. Therefore the AAM pores stay completely filled, and the structure is not distorted. A typical SAXS pattern for the cubic structure is presented in Figure 4A for the sample AAM-Cub-180. This pattern can be indexed according to the cubic  $Im\bar{3}m$  unit cell in Figure 4B, showing only reflections perpendicular to two possible zone axes,  $[01\bar{1}]$  and the  $[11\bar{2}]$ . The TEM cross section in Figure 4C of a membrane after pyrolysis at  $400\text{ }^{\circ}\text{C}$  confirms the cubic structure with the two different orientations. The FFT inset is a combination of both orientations and shows peaks at positions corresponding to the SAXS diffraction pattern. For block copolymers there are thin films known where two different structures are coexisting:

one close to the interface and a second one on top. Stein et al.<sup>45,46</sup> showed that the thickness-dependent packing results from a competition between the packing preferred in the bulk with that at the interfaces. A similar effect was found by Vogt et al.<sup>47</sup> for mesoporous carbon films. For the nanostructured carbon in the pores in the AAMs, we have a change of orientation between pore walls and the center of the pores.

**Structure Formation by Thermally Induced Self-Assembly.** The structure formation by thermally induced self-assembly could be monitored in situ for all four systems. Exemplary in situ GISAXS measurements for thin films (Film-Hex-100) and in AAMs (AAM-Hex-130) are depicted in Figure 5 and Figure 6, respectively. The remaining GISAXS data are presented in the Supporting Information, Figures S3–7 (Film-Hex-T), S9–14 (Film-Or-T), S16–21 (AAM-Hex-T), and S24–30 (AAM-Cub-T) for temperatures between  $90$  and  $220\text{ }^{\circ}\text{C}$ . In the first picture in Figure 5 (0.0 min) only specular intensities and diffuse scattering along the vertical axis are visible, thus no periodic structure is formed yet. The maxima along the vertical axis result from the staggered arrangement of multiple layers of aluminum foil acting as absorber.

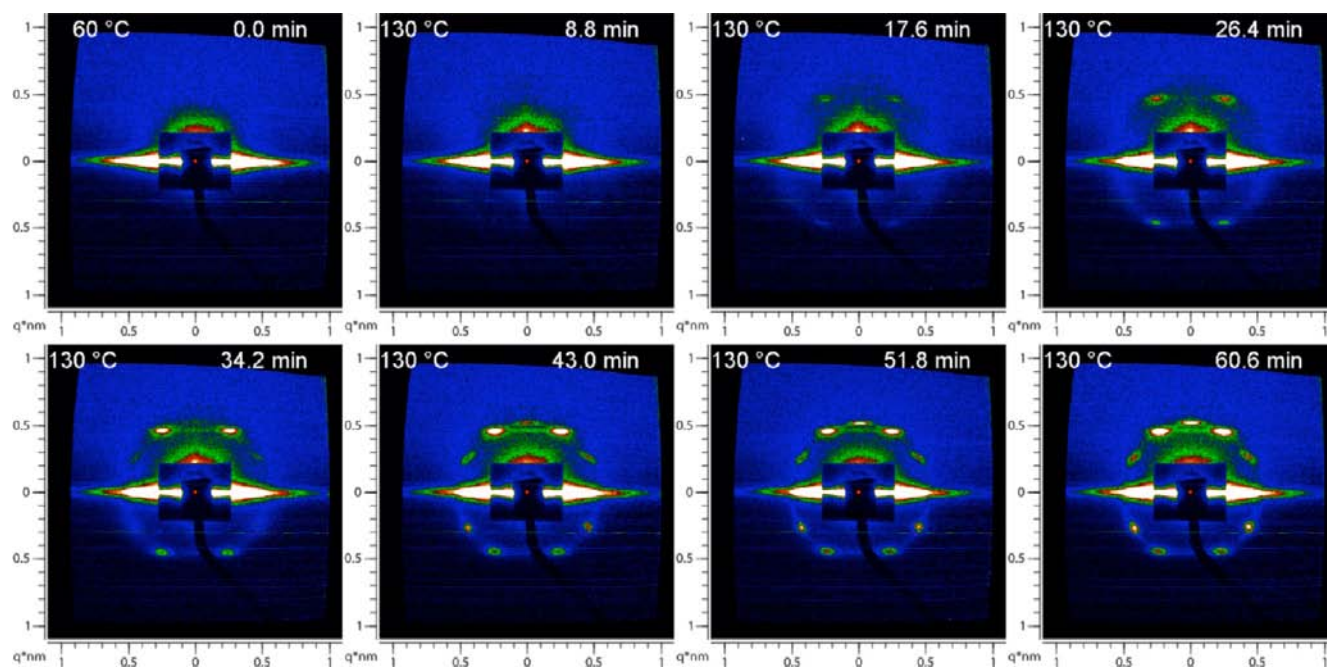


**Figure 6.** In situ SAXS of AAM-Hex-130: Structure formation during thermopolymerization at 130 °C.

Therefore, the reflections on the vertical axis (e.g.,  $d_{01}$ ) cannot be observed. After a few minutes a diffuse ring and Yoneda reflections<sup>48</sup> become visible and increase in intensity, due to an evolving mesostructure, which is oriented randomly at that stage. During continued heating, the evolution of distinct reflections related to an oriented hexagonal mesostructure occurs between 25 and 40 min after starting the heating at 60 °C. After 60 min, the reflections became more distinct and intense, but no further structural changes were visible. Remarkably, the time of structural evolution is much shorter than the well-established thermopolymerization time of 24 h used for bulk samples and films.<sup>9,14</sup>

The processes in the thermally induced structure formation in AAMs are illustrated for AAM-Hex-130 in Figure 6. After heating for 15 min at 130 °C, the first reflections related to a circular hexagonal structure start to appear. A diffuse ring attributed to worm-like phases is also visible, thus some parts are oriented randomly, while others already show the final orientation. Upon further heating the intensity of the reflection spots increases, and the structure becomes completely circular hexagonal. Some additional reflections appear after 39 min, corresponding to a hexagonally ordered top-layer on the membrane. Figure 7 summarizes the thermopolymerization process for all four OMC systems. Figure 7A shows the structural evolution for Film-Hex-100 as plot of radially integrated intensities. The maximum of out-of plane intensity ( $d_{10}$  reflection) is moving to smaller  $q$ -values until 60 min after the start and stays constant even after cooling down. This indicates a swelling of the micelles during structure formation and condensation and therefore larger  $d$ -spacings of the oriented hexagonal mesostructure compared to the randomly oriented phase. The same effect could be observed for AAM-Hex-130 in Figure 7B.

The intensity is increasing, and at the same time, the maximum shifts to smaller  $q$ -values (inset). The minimum temperature to obtain highly ordered mesostructures within a few hours was 100 °C for all four systems. At higher temperatures up to 220 °C the structure formation was much

faster. Figure 7C illustrates the observed decrease of the time for the first structure formation with increasing thermopolymerization temperature for thin films (bottom) and for AAMs (top).

The thermopolymerization times for the thin films Film-Hex-T and Film-Or-T were between 25 and 4 min, the lower limit being caused by the relatively slow heating ramp of 20 °C/min. For temperatures above 140 °C the reflections can be observed before the desired temperature is reached at this heating rate. Figure S7, Supporting Information shows an in situ GISAXS measurement (Film-Hex-180fast), where the film was heated with a ramp of 100 °C/min; here the structure formation started already after 1.6 min.

The thermopolymerization times for the samples AAM-Hex-T and AAM-Cub-T are also shorter at higher temperatures, but compared to thin films, the structure formation is much slower. This effect of the tubular confinement is attributed to higher surface energies of the resulting mesophase. Apparently, the block copolymers cannot form the phase with the lowest energy, but they have to allow circular distortion because the block copolymers have to adapt to the curved alumina surface. We note that this effect should be strong for the investigated mesophases due to their relatively large unit cells (constants between 13 and 21 nm) compared to the tubular pores (ca. 200 nm in diameter).

It appears that the structure formation for orthorhombic films is faster than the formation of the hexagonal films at equal thermopolymerization temperatures and that the cubic phase forms faster than the hexagonal phase in AAMs, which is probably caused by the different surfactants used. In both cases, OMC phases made from Pluronic F127 form faster than with Pluronic P123.

Interestingly, the final patterns for different thermopolymerization temperatures are also slightly different concerning the positions of the reflection spots, which is shown in Figure 7D for Film-Hex-T (bottom) and AAM-Hex-T (top). Higher thermopolymerization temperatures result in larger  $d$ -spacings—the reflections move closer to the beam center. Thus the

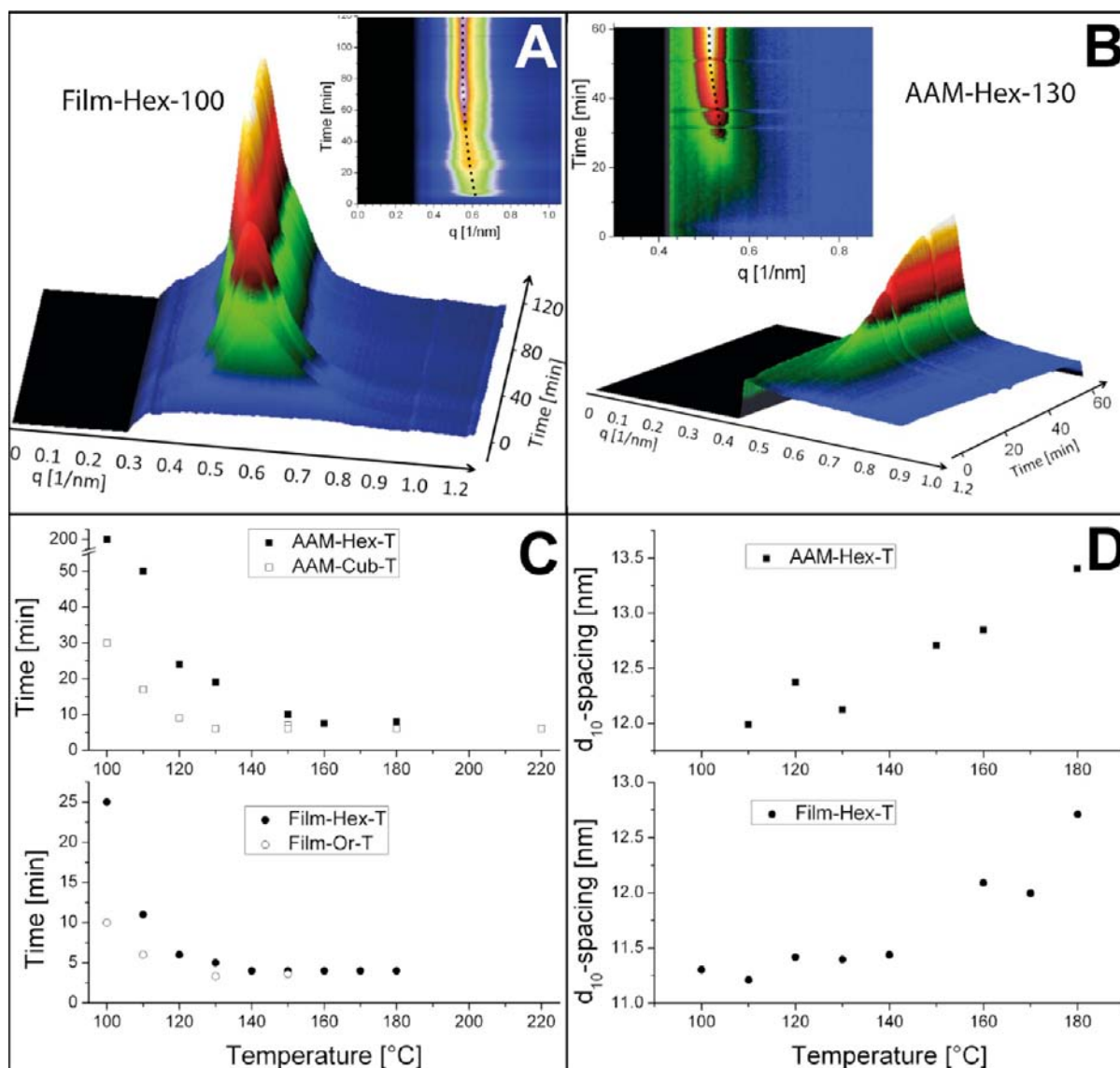


**Figure 7.** Evolution of structure during thermopolymerization. (A) Plot of thermopolymerization time vs radially integrated intensities for Film-Hex-100 in 3D projection with an inset of the 2D projection. In-plane intensity (on the vertical axis) was masked due to extremely high intensities from specular and diffuse scattering according to Figure S2A, Supporting Information. (B) Plot of thermopolymerization time vs radially integrated intensities for AAM-Hex-130. (C) Time of structure formation for samples AAM-Hex-T and AAM-Cub-T (top) and Film-Hex-T and Film-Or-T (bottom). Time (start of the 20 °C/min ramp at 60 °C until the first  $d_{10}$  or  $d_{111}$  reflections can be observed) vs the final thermopolymerization temperature. (D) The  $d_{10}$ -spacings after thermopolymerization for the samples AAM-Hex-T (top) and Film-Hex-T (bottom).

swelling effect during structure formation and condensation shown in Figure 7A,B is temperature dependent. We explain this effect by thermal expansion of the liquid crystalline block-copolymer phase during structure formation, which is then fixed in its dimensions due to condensation of the precursor oligomers in the walls. Thermal expansion of block copolymers was also investigated for smectic phases of diblock copolymers with polyethylene oxide and polymethacrylate with azobenzene blocks (PEOm-*b*-PMA(Az)).<sup>49</sup>

While for Film-Hex-T (Figure 7D, bottom) the changes between 100 and 140 °C are negligible ( $d_{10} \sim 11.4$  nm), a significant increase of the  $d_{10}$   $d$ -spacings can be observed between 160 and 180 °C, reaching 12.7 nm. The larger  $d$ -spacings result from smaller  $q(y)$  wavevectors, while the  $q(z)$  values remain constant (Figure S8A,B, Supporting Information). Thus the corresponding unit cells differ mainly in the substrate plane ( $xy$  plane) and not perpendicular to it

( $z$  direction). This effect could be caused by a compensation of the swelling liquid crystal phase and uniaxial ( $z$ ) shrinkage of the resol network. For AAM-Hex-T (Figure 7D, top) we show the shift of the 10 reflection to lower angles with increasing thermopolymerization temperature; the distribution into  $y$  and  $z$  components is shown in Figure S22, Supporting Information. Both the  $q(y)$  and  $q(z)$  values decrease with higher thermopolymerization temperatures. The decreasing  $q(y)$  reveals larger lattice plane distances parallel to the membrane wall, while the  $q(z)$  values show stretched  $d$ -spacings along the membrane normal. The differences are up to 10% in both cases. This shows swelling of the complete unit cells of the liquid crystal structures during structure formation with increasing thermopolymerization temperatures but no significant distortion. The final mesostructures of the samples AAM-Cub-T also differ in unit cell parameters. Figure S31, Supporting Information depicts the  $d$ -spacing of the  $10\bar{1}$  reflection

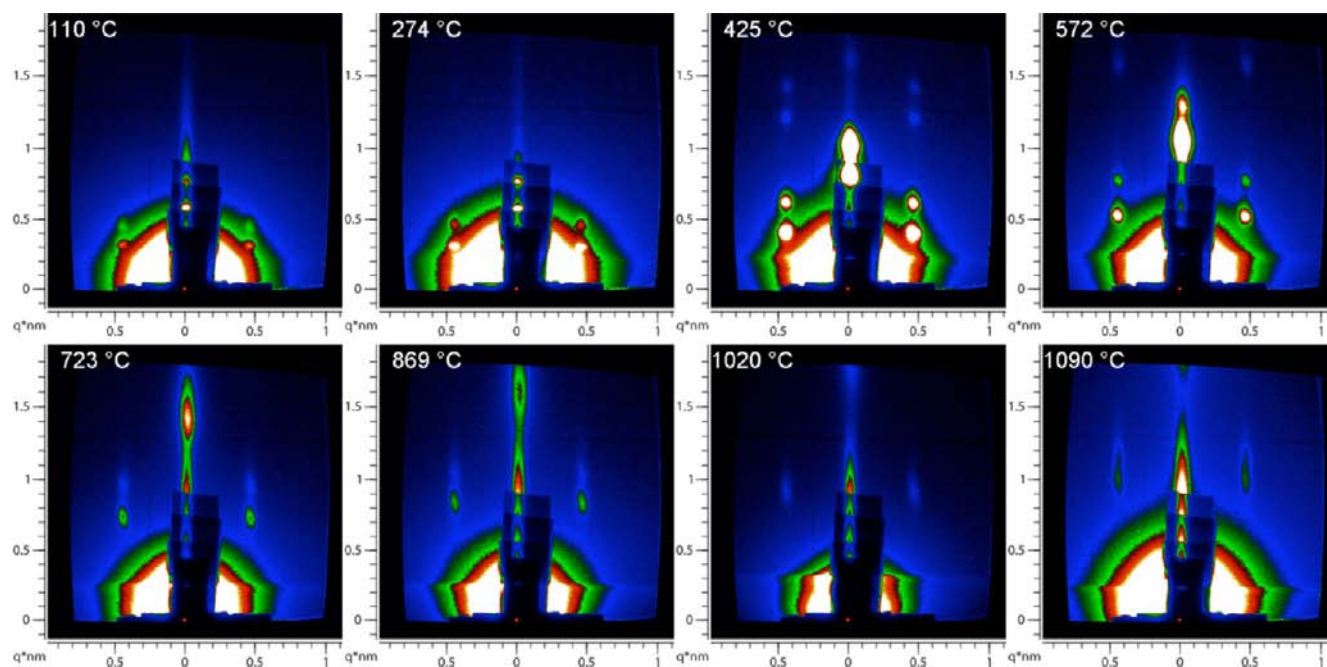


**Figure 8.** Carbonization of Film-Hex-110 presented in a series of GISAXS patterns. The most intense reflections are doubled due to the grazing incidence geometry (the lower reflection results from Bragg diffraction, and the second reflection on top of the first one is a specular reflection of the corresponding Bragg reflection). The strongly increased diffuse scattering as compared to the patterns in Figure 1 stems from the graphite dome on the heating chamber. Directions:  $q(z)$ : vertical;  $q(y)$ : horizontal.

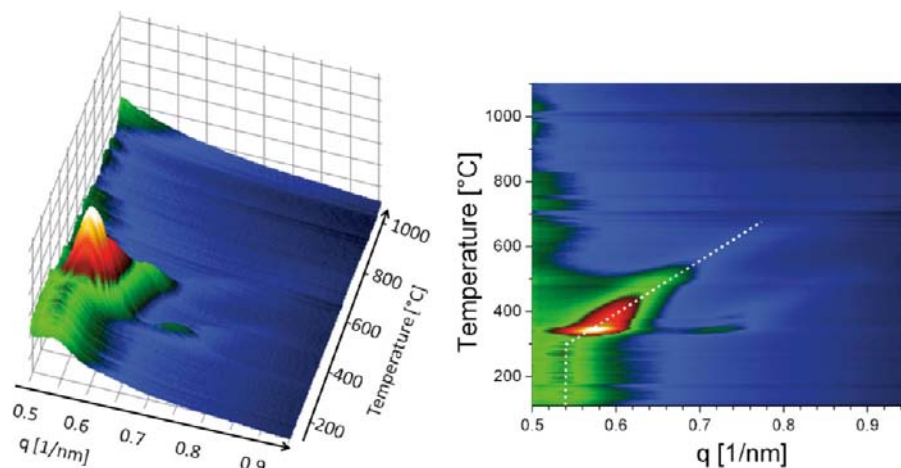


**Figure 9.** Carbonization of Film-Hex-110 as plot of the radial intensities: Plot of carbonization temperature vs radially integrated intensities (3D: left; 2D: right, in-plane intensity and intensity from scattering of the graphite dome are masked according to Figure S2B, Supporting Information). The main intensity is related to the 10-reflection. The dotted line indicates the position of the reflection maximum.

(perpendicular to  $[11\bar{2}]$ ), which is shifted to lower angles with increasing thermopolymerization temperature. The same trend as for the circular hexagonal phase is visible here; the  $d$ -spacings grow larger for higher thermopolymerization temperatures due to swelling of the liquid crystal mesostructures during thermopolymerization.

One explanation for the mechanism of thermally induced self-assembly can be increased segregation strength due to polymerization of the resol oligomers. Watkins et al.<sup>38</sup> showed that adding poly(acrylic acid) (PAA) as polymer results in an ordered structure. In contrast, upon addition of monomeric 1-propanoic acid the structure remained disordered, although the interaction enthalpy with the ether oxygen should be similar. In this study the initial resol oligomers polymerize at elevated

temperatures, which could increase the segregation strength in a similar way. Alternatively, the material could be simply kinetically locked at low temperatures. In this case, the observed thermally induced self-assembly would be based on increased kinetics due to heating. As the polymerization rate and the kinetics of polymer diffusion increase with increasing temperature, none of the above explanations can be excluded here, and a combination of both is also possible. As thermopolymerization and structure formation take place at around the same temperature, the explanation based on increased segregation strength due to polymerization seems to be more likely. The mechanism of thermally induced structure formation was already confirmed by a subsequent study.<sup>50</sup> There it was shown that this process is not limited to

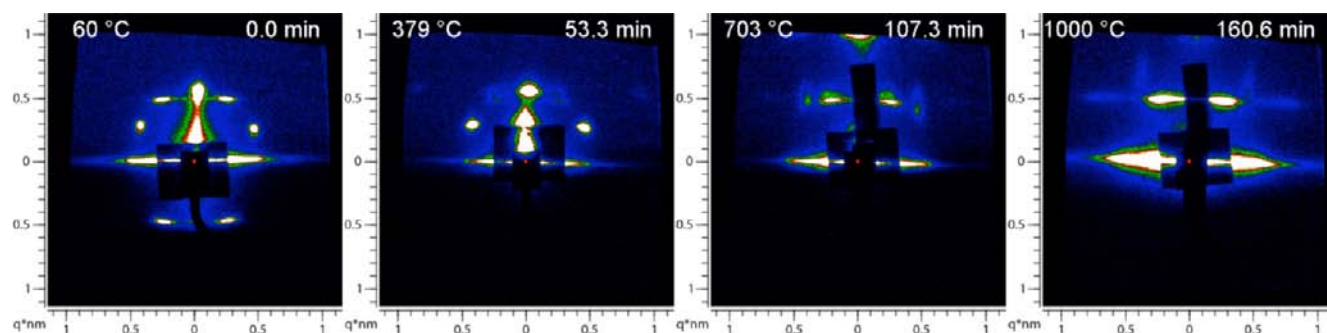


**Figure 10.** Carbonization of AAM-Hex-100: The reflections related to the top layer are moving due to shrinkage and vanish completely. In contrast, the reflections originating from the mesophase in the AAM pores do not shift; the shrinkage is restricted due to the confinement effect.

the Pluronic/resol system; it was also found for the PS-*b*-PEO/resol system.

**Carbonization.** The carbonization of a thin film is illustrated for sample Film-Hex-110 during heating in nitrogen to 1090 °C (ramp of 6 °C/min) with a series of GISAXS patterns in Figure 8 and a plot of radially integrated intensities in Figure 9. In Figure 8 we observe parallel movement of the reflections along  $q(z)$ , demonstrating the uniaxial shrinkage of the pore system along the substrate normal during carbonization. The first changes to the initial mesostructure are visible at around 330 °C, subsequently the intensity of the reflections increases drastically and higher order reflections arise, due to template removal and the resulting greater contrast in electron density. The reflections also shift to higher  $q$ -values along the vertical axis due to unit cell shrinkage perpendicular to the surface of the film. The intensity plot in Figure 9 shows that the maximum intensity is already reached around 350 °C, where the structure is only slightly distorted. At higher temperatures the reflection intensity decreases strongly while continuously shifting to higher  $q(z)$ -values. These observations show that the structure becomes less ordered at higher carbonization temperature. The reflections of the mesostructure remain visible up to 1090 °C (Figure 8), thus the mesostructure did not collapse completely. We note that the structure is retained at the high temperatures due to the relatively fast heating ramp of 6 °C/min; low ramp rates, such as 1 °C/min, will lead to structural collapse at lower temperatures.<sup>14</sup> The pyrolysis for phenolic resins consists of several reactions<sup>51</sup> taking place at different temperatures. They could all lead to structural changes due to mass loss and reduction of surface area and therefore have a critical impact on the collapse of the mesostructural order. Thus, the ramp rate can be important for the thermal stability. The carbonization process for the orthorhombic film Film-Or-100 was also followed in situ with GISAXS as depicted in Figure S15, Supporting Information. The film was heated up to 1050 °C in nitrogen with a ramp of 6 °C/min. The film shows the same behavior of uniaxial shrinkage and carbonization as the hexagonal films. Thus, the orthorhombic films can also be carbonized to highly ordered mesoporous carbon films at temperatures above 600 °C and can even resist high temperatures up to 1050 °C for several hours.

The carbonization of sample AAM-Hex-100 was monitored in situ up to 1000 °C (Figure 10, a more detailed series in Figure S23, Supporting Information).

The initial pattern shows reflections related to the circular hexagonal structure and also reflections from a top-layer (compare Figure 3). The measurement shows the carbonization of the circular hexagonal structure up to 1000 °C, the shift of

the reflections from the top layer due to shrinkage, and the restricted shrinkage effect due to the confinement of the AAM pores. It also illustrates the striking effect of confinement on the thermal stability, as the reflections from the top layer completely vanish, but the reflections from the mesostructure even increase in intensity up to 1000 °C. The carbonization of the sample AAM-Cub-100 could also be followed in situ, which is shown in Figure S32, Supporting Information. The restricted shrinkage due to confinement can also be observed here; the reflections increase drastically in intensity, and higher order reflections become visible due to template removal, but no change in position is observed due to the restricted shrinkage effect of the confining AAM pores.

## CONCLUSIONS

In this in situ SAXS study we have investigated a new mechanism for the mesostructure formation of OMC phases in confined environments: thermally induced self-assembly. The OMC phases, 2D-hexagonal and orthorhombic for thin films and cubic and circular hexagonal for anodic alumina membranes (AAMs), were obtained by organic–organic self-assembly of a preformed oligomeric resol precursor and the triblock copolymer templates Pluronic P123 and F127, respectively. Importantly, we show that unlike mesostructured metal oxides and also different to literature on those soft-templated OMCs, the structure formation for the studied OMC systems does not occur during the evaporation process but during a thermopolymerization step and can thus be called thermally induced self-assembly.

As a remarkable consequence, the mesostructure is not fixed but still flexible and can be controlled during this step. Moreover, we find that higher thermopolymerization temperatures result in increased unit cell parameters, caused by swelling of the liquid crystal structures of the block copolymer templates. Interestingly, the distortion of the unit cell for hexagonal thin films mainly originates from an increase of the cell parallel to the substrate plane and is therefore not visible in standard detector scans. We also find that the rate of the structure formation strongly depends on the thermopolymerization temperature and on the block copolymer template. Template removal and carbonization of thin films and AAMs were monitored in situ up to 1100 °C, without total loss of structure. In both cases, the template decomposition started at temperatures around 330 °C, indicated by a strong intensity increase in the GISAXS patterns. Strong structural distortion of the thin films was observed due to anisotropic shrinkage. In striking contrast, the confined OMC phases in the AAM hosts

were not subject to distortion even at the high carbonization temperatures reached in this study.

The new mechanism discovered here offers additional opportunities for mesostructure control. We have demonstrated the influence of different temperatures during this thermally induced self-assembly on the final mesostructure, and we suppose that the change of other synthesis parameters, such as the vapor atmosphere, will also show significant effects and should thus be subject of further studies.

## ■ ASSOCIATED CONTENT

### Supporting Information

Masks used for radial intensity integrations, image series of in situ SAXS measurements for thermopolymerization and carbonization, and plots of  $q(y)$  and  $q(z)$  values for different thermopolymerization temperatures are presented. This material is available free of charge via the Internet at <http://pubs.acs.org>.

## ■ AUTHOR INFORMATION

### Corresponding Author

bein@lmu.de

### Notes

The authors declare no competing financial interest.

## ■ ACKNOWLEDGMENTS

The authors thank the DFG (Nanosystems Initiative Munich Cluster (NIM) and SFB 486) as well as CeNS for their support of this work. Beam time at the synchrotron Elettra (Trieste, Italy) is gratefully acknowledged. We thank Andreas Zürner, Yan Li, Bettina Lotsch, Johann Szeifert, and Benjamin Mandlmeier for assistance at the synchrotron.

## ■ REFERENCES

- (1) Liang, C.; Li, Z.; Dai, S. *Angew. Chem., Int. Ed.* **2008**, *47*, 3696.
- (2) Chang, H.; Joo, S. H.; Pak, C. J. *Mater. Chem.* **2007**, *17*, 3078.
- (3) Wan, Y.; Shi, Y.; Zhao, D. *Chem. Mater.* **2008**, *20*, 932.
- (4) Wu, C.-G.; Bein, T. *Science* **1994**, *266*, 1013.
- (5) Lee, J.; Yoon, S.; Hyeon, T.; Oh, S. M.; Kim, K. B. *Chem. Commun.* **1999**, 2177.
- (6) Ryoo, R.; Joo, S. H.; Jun, S. J. *Phys. Chem. B* **1999**, *103*, 7743.
- (7) Jun, S.; Joo, S. H.; Ryoo, R.; Kruk, M.; Jaroniec, M.; Liu, Z.; Ohsuna, T.; Terasaki, O. *J. Am. Chem. Soc.* **2000**, *122*, 10712.
- (8) Kruk, M.; Jaroniec, M.; Kim, T.-W.; Ryoo, R. *Chem. Mater.* **2003**, *15*, 2815.
- (9) Meng, Y.; Gu, D.; Zhang, F.; Shi, Y.; Cheng, L.; 34, D.; Wu, Z.; Chen, Z.; Wan, Y.; Stein, A.; Zhao, D. *Chem. Mater.* **2006**, *18*, 4447.
- (10) Lu, A.-H.; Spliethoff, B.; Schueth, F. *Chem. Mater.* **2008**, *20*, 5314.
- (11) Wang, X.; Liang, C.; Dai, S. *Langmuir* **2008**, *24*, 7500.
- (12) Liang, C.; Hong, K.; Guiochon, G. A.; Mays, J. W.; Dai, S. *Angew. Chem., Int. Ed.* **2004**, *43*, 5785.
- (13) Tanaka, S.; Katayama, Y.; Tate, M. P.; Hillhouse, H. W.; Miyake, Y. *J. Mater. Chem.* **2007**, *17*, 3639.
- (14) Schuster, J.; Koehn, R.; Keilbach, A.; Doeblinger, M.; Amenitsch, H.; Bein, T. *Chem. Mater.* **2009**, *21*, 5754.
- (15) Song, L.; Feng, D.; Fredin, N. J.; Yager, K. G.; Jones, R. L.; Wu, Q.; Zhao, D.; Vogt, B. D. *ACS Nano* **2009**, *4*, 189.
- (16) Song, L.; Feng, D.; Campbell, C. G.; Gu, D.; Forster, A. M.; Yager, K. G.; Fredin, N.; Lee, H.-J.; Jones, R. L.; Zhao, D.; Vogt, B. D. *J. Mater. Chem.* **2010**, *20*, 1691.
- (17) Zheng, M.; Cao, J.; Ke, X.; Ji, G.; Chen, Y.; Shen, K.; Tao, J. *Carbon* **2007**, *45*, 1111.
- (18) Steinhart, M.; Liang, C.; Lynn, G. W.; Goesele, U.; Dai, S. *Chem. Mater.* **2007**, *19*, 2383.

- (19) Wang, K.; Zhang, W.; Phelan, R.; Morris, M. A.; Holmes, J. D. *J. Am. Chem. Soc.* **2007**, *129*, 13388.
- (20) Wang, K.; Birjukovs, P.; Erts, D.; Phelan, R.; Morris, M. A.; Zhou, H.; Holmes, J. D. *J. Mater. Chem.* **2009**, *19*, 1331.
- (21) Zheng, M.; Ji, G.; Wang, Y.; Cao, J.; Feng, S.; Liao, L.; Du, Q.; Zhang, L.; Ling, Z.; Liu, J.; Yu, T.; Cao, J.; Tao, J. *Chem. Commun.* **2009**, 5033.
- (22) Tanaka, S.; Doi, A.; Nakatani, N.; Katayama, Y.; Miyake, Y. *Carbon* **2009**, *47*, 2688.
- (23) Schuster, J.; Keilbach, A.; Köhn, R.; Döblinger, M.; Dörfler, T.; Dennenwaldt, T.; Bein, T. *Chem.–Eur. J.* **2011**, *17*, 9463.
- (24) Cott, D. J.; Petkov, N.; Morris, M. A.; Platschek, B.; Bein, T.; Holmes, J. D. *J. Am. Chem. Soc.* **2006**, *128*, 3920.
- (25) Pang, J.; Li, X.; Wang, D.; Wu, Z.; John, V. T.; Yang, Z.; Lu, Y. *Adv. Mater.* **2004**, *16*, 884.
- (26) Brinker, C. J.; Lu, Y.; Sellinger, A.; Fan, H. *Adv. Mater.* **1999**, *11*, 579.
- (27) Grosso, D.; Babonneau, F.; Albouy, P.-A.; Amenitsch, H.; Balkenende, A. R.; Brunet-Bruneau, A.; Rivory, J. *Chem. Mater.* **2002**, *14*, 931.
- (28) Platschek, B.; Koehn, R.; Doeblinger, M.; Bein, T. *Langmuir* **2008**, *24*, 5018.
- (29) Falcaro, P.; Grosso, D.; Amenitsch, H.; Innocenzi, P. *J. Phys. Chem. B* **2004**, *108*, 10942.
- (30) Smarsly, B.; Grosso, D.; Brezesinski, T.; Pinna, N.; Boissière, C.; Antonietti, M.; Sanchez, C. *Chem. Mater.* **2004**, *16*, 2948.
- (31) Yan, Y.; Zhang, F.; Meng, Y.; Tu, B.; Zhao, D. *Chem. Commun.* **2007**, 2867.
- (32) Geranmayeh, S.; Abbasi, A.; Badiei, A. *E-J. Chem.* **2011**, *8*, 196.
- (33) Meng, Y.; Gu, D.; Zhang, F.; Shi, Y.; Yang, H.; Li, Z.; Yu, C.; Tu, B.; Zhao, D. *Angew. Chem., Int. Ed.* **2005**, *44*, 7053.
- (34) Feng, D.; Lv, Y.; Wu, Z.; Dou, Y.; Han, L.; Sun, Z.; Xia, Y.; Zheng, G.; Zhao, D. *J. Am. Chem. Soc.* **2011**, *133*, 15148.
- (35) Leiston-Belanger, J. M.; Russell, T. P.; Drockenmuller, E.; Hawker, C. J. *Macromolecules* **2005**, *38*, 7676.
- (36) Jang, S. G.; Kim, B. J.; Hawker, C. J.; Kramer, E. J. *Macromolecules* **2011**, *44*, 9366.
- (37) Bates, F. S.; Fredrickson, G. H. *Annu. Rev. Phys. Chem.* **1990**, *41*, 525.
- (38) Tirumala, V. R.; Daga, V.; Bosse, A. W.; Romang, A.; Ilavsky, J.; Lin, E. K.; Watkins, J. J. *Macromolecules* **2008**, *41*, 7978.
- (39) Daga, V. K.; Watkins, J. J. *Macromolecules* **2010**, *43*, 9990.
- (40) Amenitsch, H.; Rappolt, M.; Kriechbaum, M.; Mio, H.; Laggner, P.; Bernstorff, S. *Journal of Synchrotron Radiation* **1998**, *5*, 506.
- (41) Tate, M. P.; Urade, V. N.; Kowalski, J. D.; Wei, T.-c.; Hamilton, B. D.; Eggiman, B. W.; Hillhouse, H. W. *J. Phys. Chem. B* **2006**, *110*, 9882.
- (42) Ghiorso, M.; Carmichael, I.; Moret, L. *Contrib. Mineral. Petrol.* **1979**, *68*, 307.
- (43) Tucker, M. G.; Keen, D. A.; Dove, M. T. *Mineral. Mag.* **2001**, *65*, 489.
- (44) Tate, M. P.; Urade, V. N.; Kowalski, J. D.; Wei, T.-c.; Hamilton, B. D.; Eggiman, B. W.; Hillhouse, H. W. *J. Phys. Chem. B* **2006**, *110*, 9882.
- (45) Stein, G. E.; Cochran, E. W.; Katsov, K.; Fredrickson, G. H.; Kramer, E. J.; Li, X.; Wang, J. *Phys. Rev. Lett.* **2007**, *98*, 158302.
- (46) Stein, G. E.; Kramer, E. J.; Li, X.; Wang, J. *Macromolecules* **2007**, *40*, 2453.
- (47) Vogt, B. D.; Chavez, V. L.; Dai, M.; Arreola, M. R. C.; Song, L.; Feng, D.; Zhao, D.; Perera, G. M.; Stein, G. E. *Langmuir* **2011**, *27*, 5607.
- (48) Yoneda, Y. *Phys. Rev.* **1963**, *131*, 2010.
- (49) Watanabe, R.; Iyoda, T.; Yamada, T.; Yoshida, H. *J. Therm. Anal. Calorim.* **2006**, *85*, 713.
- (50) Labiano, A.; Dai, M.; Young, W.-S.; Stein, G. E.; Cavicchi, K. A.; Epps, T. H.; Vogt, B. D. *J. Phys. Chem. C* **2012**, *116*, 6038.
- (51) Trick, K. A.; Saliba, T. E. *Carbon* **1995**, *33*, 1509.